Detecting cosmic bubble collisions with optimal filters

Jason McEwen[1,*], Stephen Feeney[1], Matthew Johnson[2], Hiranya Peiris[1]

[*] http://www.jasonmcewen.org/

[1] *Department of Physics and Astronomy, University College London (UCL), UK*

[2] *Perimeter Institute for Theoretical Physics, Canada*

Preprint arXiv:1202.2861

47th Rencontres de Moriond :: March 2012

Outline

Slow-roll inflation

- Inflation: period of exponential expansion in the very early Universe.
- Strong observational evidence for inflation.
- Standard/simplest descriptions of inflation are slow-roll.
- However, this is a phenomenological description only and is not well motivated.
- We would like inflation to be a consequence of high-energy physics!

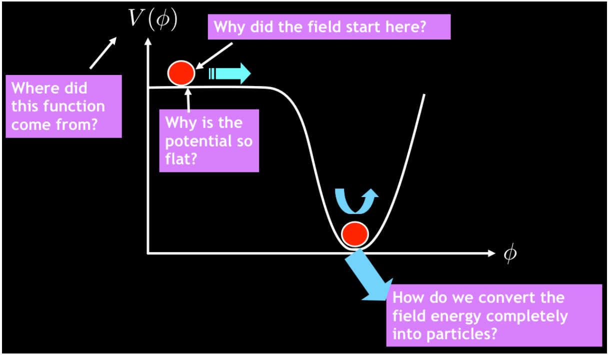

Slow-roll inflation

- Inflation: period of exponential expansion in the very early Universe.
- Strong observational evidence for inflation.
- Standard/simplest descriptions of inflation are slow-roll.
- However, this is a phenomenological description only and is not well motivated.
- **We would like inflation to be a consequence of high-energy physics!**

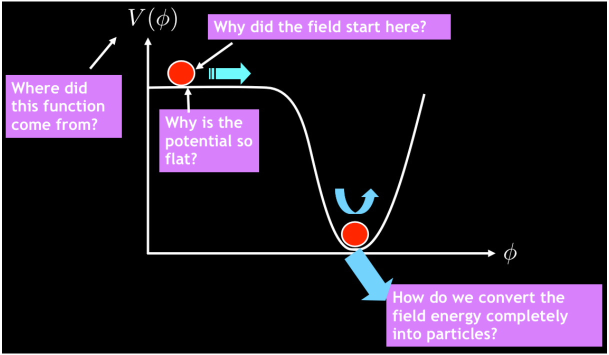

Eternal inflation

- Theories of inflation with a unique vacuum are difficult to come by.
- For example, string theories give landscape of 4D vacua, all of which are occupied.
- Field trapped in false vacuum $\Rightarrow$ inflates forever!

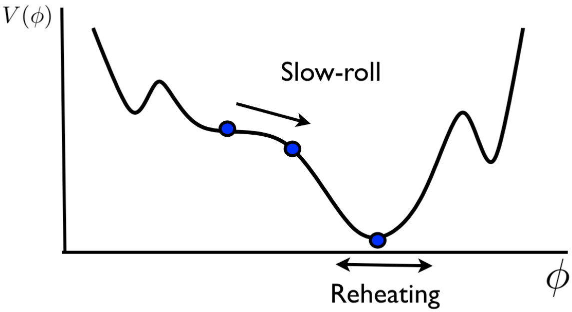

Eternal inflation

- Theories of inflation with a unique vacuum are difficult to come by.
- For example, string theories give landscape of 4D vacua, all of which are occupied.
- Field trapped in false vacuum $\Rightarrow$ inflates forever!
- Tunnelling creates a bubble!
- If bubble nucleation rate less than bulk expansion, then inflation is eternal.

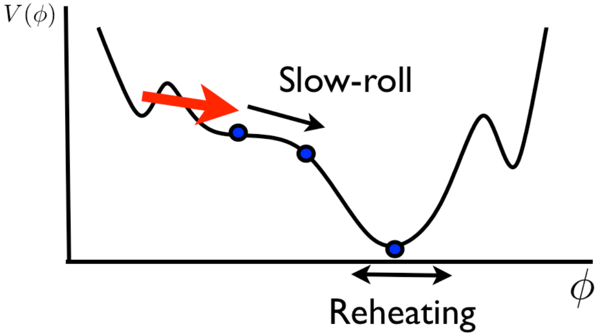

Eternal inflation

- Theories of inflation with a unique vacuum are difficult to come by.
- For example, string theories give landscape of 4D vacua, all of which are occupied.
- Field trapped in false vacuum $\Rightarrow$ inflates forever!
- Tunnelling creates a bubble!
- If bubble nucleation rate less than bulk expansion, then inflation is eternal.

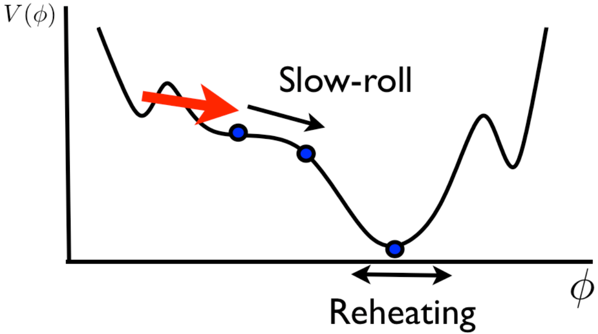

Bubble universes

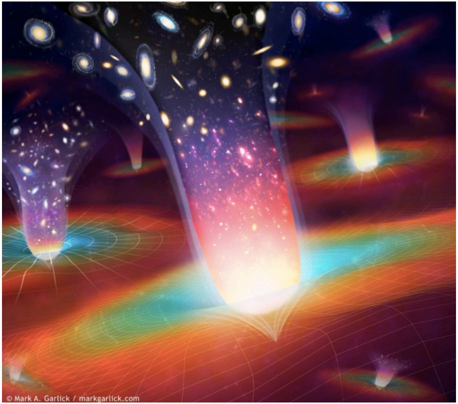

Bubble collisions

- Bubble collisions may have left observational signatures in the CMB.

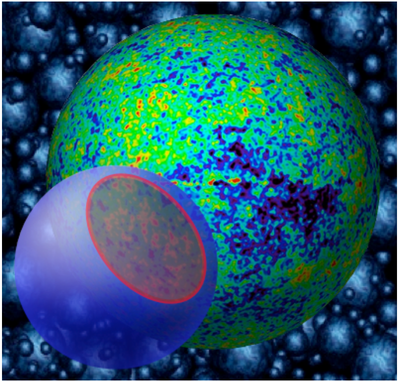

Bubble collisions

- Bubble collisions may have left observational signatures in the CMB.

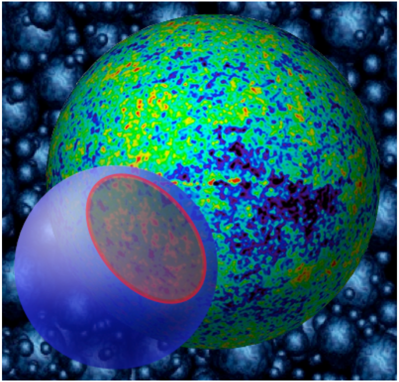

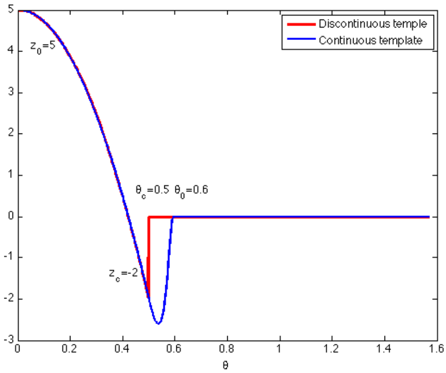

Full-sky object detection

- Bayesian object detection would provide a rigorous statistical framework for comparing models with differing numbers of bubble collisions.
- However, such an analysis is computationally intractable!
  - Requires the inversion of a **3 million** $\times$ **3 million** matrix for WMAP data.
  - Requires the inversion of a **50 million** $\times$ **50 million** matrix for Planck data.
- Alternatively, perform a preprocessing to detect candidate bubble collisions, followed by a local Bayesian analysis.
- This approach has been pioneered by Feeney *et al.* (2011a,2011b), using wavelets (needlets) on the sphere.
- However, we know signature of candidate bubble collisions $\rightarrow$ exploit this knowledge!
- Build optimal filters tailored to the expected bubble collision signatures.
- Replace the wavelet (needlet) preprocessing stage with optimal filters.

Full-sky object detection

- Bayesian object detection would provide a rigorous statistical framework for comparing models with differing numbers of bubble collisions.
- However, such an analysis is computationally intractable!
  - Requires the inversion of a **3 million** $\times$ **3 million** matrix for WMAP data.
  - Requires the inversion of a **50 million** $\times$ **50 million** matrix for Planck data.
- Alternatively, perform a preprocessing to detect candidate bubble collisions, followed by a local Bayesian analysis.
- This approach has been pioneered by Feeney *et al.* (2011a,2011b), using wavelets (needlets) on the sphere.
- However, we know signature of candidate bubble collisions $\rightarrow$ exploit this knowledge!
- Build optimal filters tailored to the expected bubble collision signatures.
- Replace the wavelet (needlet) preprocessing stage with optimal filters.

Full-sky object detection

- Bayesian object detection would provide a rigorous statistical framework for comparing models with differing numbers of bubble collisions.
- However, such an analysis is computationally intractable!
  - Requires the inversion of a **3 million** $\times$ **3 million** matrix for WMAP data.
  - Requires the inversion of a **50 million** $\times$ **50 million** matrix for Planck data.
- Alternatively, perform a preprocessing to detect candidate bubble collisions, followed by a local Bayesian analysis.
- This approach has been pioneered by Feeney *et al.* (2011a,2011b), using wavelets (needlets) on the sphere.
- However, we know signature of candidate bubble collisions $\rightarrow$ exploit this knowledge!
- Build optimal filters tailored to the expected bubble collision signatures.
- Replace the wavelet (needlet) preprocessing stage with optimal filters.

Full-sky object detection

- Bayesian object detection would provide a rigorous statistical framework for comparing models with differing numbers of bubble collisions.
- However, such an analysis is computationally intractable!
  - Requires the inversion of a **3 million** $\times$ **3 million** matrix for WMAP data.
  - Requires the inversion of a **50 million** $\times$ **50 million** matrix for Planck data.
- Alternatively, perform a preprocessing to detect candidate bubble collisions, followed by a local Bayesian analysis.
- This approach has been pioneered by Feeney *et al.* (2011a,2011b), using wavelets (needlets) on the sphere.
- However, we know signature of candidate bubble collisions $\rightarrow$ exploit this knowledge!
- Build optimal filters tailored to the expected bubble collision signatures.
- Replace the wavelet (needlet) preprocessing stage with optimal filters.

Filtering for full-sky object detection

- The observed field may be represented by

$$y(\omega) = \sum_i s_i(\omega) + n(\omega) \ .$$

- Each source may be represented in terms of its amplitude A_i and source profile:

$$s_i(\omega) = A_i \ \tau_i(\omega)$$

where $\tau_i(\omega)$ is a dilated and rotated version of the source profile $\tau(\omega)$ of default dilation centred on the north pole, *i.e.* $\tau_i(\omega) = \mathcal{R}(\rho_i) \ \mathcal{D}(R_i|p) \ \tau(\omega)$.

- One wishes to recover the parameters $\{A_i, R_i, \rho_i\}$ that describe each source amplitude, scale and position/orientation respectively.

- Filter the signal on the sphere to enhance the source profile relative to the background noise process $n(\omega)$:

$$\boxed{w(\rho, R|p) = \int_{S^2} d\Omega(\omega) \, f(\omega) \, [\mathcal{R}(\rho)\Psi_{R|p}]^*(\omega) \ ,}$$

where $\Psi \in L^2(S^2, d\Omega(\omega))$ is the filter kernel and p denotes the p-norm that the scaling R is defined to perserve.

Filtering for full-sky object detection

- The observed field may be represented by

$$y(\omega) = \sum_i s_i(\omega) + n(\omega) \; .$$

- Each source may be represented in terms of its amplitude A_i and source profile:

$$s_i(\omega) = A_i \; \tau_i(\omega)$$

  where $\tau_i(\omega)$ is a dilated and rotated version of the source profile $\tau(\omega)$ of default dilation centred on the north pole, *i.e.* $\tau_i(\omega) = \mathcal{R}(\rho_i) \; \mathcal{D}(R_i|p) \; \tau(\omega)$.

- One wishes to recover the parameters $\{A_i, R_i, \rho_i\}$ that describe each source amplitude, scale and position/orientation respectively.

- Filter the signal on the sphere to enhance the source profile relative to the background noise process $n(\omega)$:

$$\boxed{w(\rho, R|p) = \int_{S^2} \mathrm{d}\Omega(\omega) \; f(\omega) \; [\mathcal{R}(\rho) \Psi_{R|p}]^*(\omega) \; ,}$$

  where $\Psi \in L^2(S^2, \mathrm{d}\Omega(\omega))$ is the filter kernel and p denotes the p-norm that the scaling R is defined to perserve.

Filtering for full-sky object detection

- The observed field may be represented by

$$y(\omega) = \sum_i s_i(\omega) + n(\omega) \; .$$

- Each source may be represented in terms of its amplitude A_i and source profile:

$$s_i(\omega) = A_i \; \tau_i(\omega)$$

 where $\tau_i(\omega)$ is a dilated and rotated version of the source profile $\tau(\omega)$ of default dilation centred on the north pole, *i.e.* $\tau_i(\omega) = \mathcal{R}(\rho_i) \; \mathcal{D}(R_i|p) \; \tau(\omega)$.

- One wishes to recover the parameters $\{A_i, R_i, \rho_i\}$ that describe each source amplitude, scale and position/orientation respectively.
- Filter the signal on the sphere to enhance the source profile relative to the background noise process $n(\omega)$:

$$\boxed{w(\rho, R|p) = \int_{\mathrm{S}^2} \mathrm{d}\Omega(\omega) \, f(\omega) \; [\mathcal{R}(\rho) \Psi_{R|p}]^* (\omega) \; ,}$$

where $\Psi \in L^2(\mathrm{S}^2, \; \mathrm{d}\Omega(\omega))$ is the filter kernel and p denotes the p-norm that the scaling R is defined to perserve.

Matched filter (MF)

- Matched filtering has been considered extensively in Euclidean space (*e.g.* the plane) to enhance a source profile in a background noise process (*e.g.* Sanz *et al.* (2001), Herranz *et al.* (2002)).
- Extend matching filtering to the sphere (JDM *et al.* (2008)).

Matched filter (MF) on the sphere

The optimal MF defined on the sphere is obtained by solving the constrained optimisation problem:

$$\min_{\text{w.r.t. } (\Psi_{R|p})_{\ell m}} \sigma_w^2(\mathbf{0}, R|p) \qquad \text{such that} \qquad \langle w(\mathbf{0}, R|p) \rangle = A \; .$$

The spherical harmonic coefficients of the resultant MF are given by

$$\boxed{(\Psi_{R|p})_{\ell m} = \frac{\tau_{\ell m}}{a \, C_\ell} \; ,}$$

where

$$a = \sum_{\ell m} C_\ell^{-1} |\tau_{\ell m}|^2 \; .$$

Scale adaptive filter (SAF)

- Scale adaptive filter derived in Euclidean space by Sanz *et al.* (2001) and Herranz *et al.* (2002), not only to enhance the source profile, but also to impose an extreme in scale.
- Extended to the sphere (JDM *et al.* (2008)).

Scale adaptive filter (SAF) on the sphere

The optimal SAF defined on the sphere is obtained by by solving the constrained optimisation problem:

$$\min_{\text{w.r.t. } (\Psi_{R_0|p})_{\ell m}} \sigma_w^2(\mathbf{0}, R|p)$$

such that

$$\langle w(\mathbf{0}, R|p)\rangle = A \quad \text{and} \quad \frac{\partial}{\partial R}\langle w(\mathbf{0}, R|p)\rangle\Big|_{R=R_0} = 0 \, .$$

The spherical harmonic coefficients of the resultant SAF are given by

$$\boxed{(\Psi_{R_0|p})_{\ell m} = \frac{c\tau_{\ell m} - b(A_{\ell p}\tau_{\ell m} - B_{\ell m}\tau_{\ell-1,m})}{\Delta C_\ell} \, ,}$$

where

$$b = \sum_{\ell m} C_\ell^{-1}\tau_{\ell m}(A_{\ell p}\tau_{\ell m}^* - B_{\ell m}\tau_{\ell-1,m}^*) \, ,$$

$$c = \sum_{\ell m} C_\ell^{-1}\left|A_{\ell p}\tau_{\ell m} - B_{\ell m}\tau_{\ell-1,m}\right|^2 \, ,$$

$\Delta = ac - |b|^2$, a is defined as before, $A_{\ell p} \equiv \ell + 2/p - 1$ and $B_{\ell m} \equiv (\ell^2 - m^2)^{1/2}$.

Optimal filters for bubble signatures

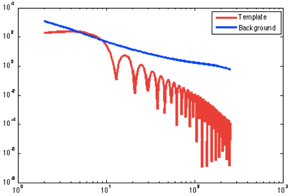

(a) Spectra

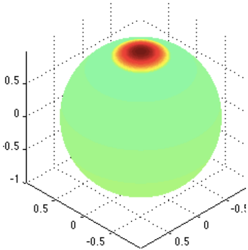

(b) Template

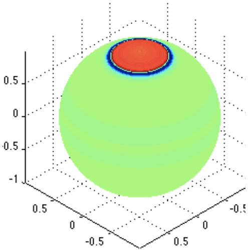

(c) MF

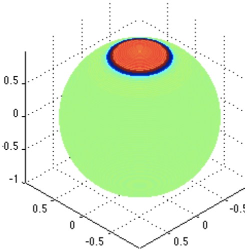

(d) SAF

Figure: Optimal filters for bubble template with size $\theta_{\rm crit} = 20^\circ$.

Optimal filters for bubble signatures

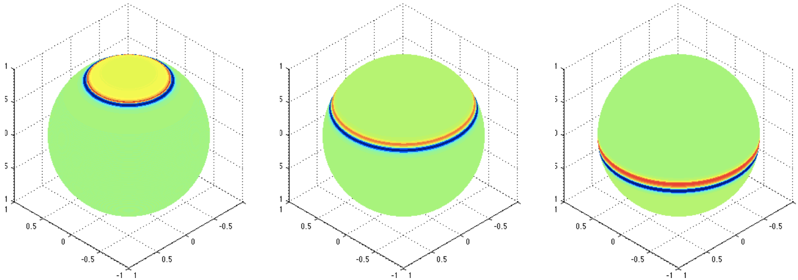

(a) $\theta_{\text{crit}} = 30^\circ$ (b) $\theta_{\text{crit}} = 60^\circ$ (c) $\theta_{\text{crit}} = 90^\circ$

Figure: MF for various template sizes

Theoretical signal-to-noise ratios (SNRs)

- Predict the expected SNR for a given filter:

$$\Gamma \equiv \frac{\langle w(\mathbf{0}, R|p) \rangle}{\sigma_w(\mathbf{0}, R|p)} \ .$$

- For the MF, SAF and an arbitrary filter Ψ we find, respectively,

$$\Gamma_{\rm MF} = a^{1/2} A \ ,$$

$$\Gamma_{\rm SAF} = c^{-1/2} \Delta^{1/2} A \ ,$$

and

$$\Gamma_{\Psi} = \frac{A \sum_{\ell m} \tau_{\ell m} \Psi^*_{\ell m}}{\sqrt{\sum_{\ell m} C_\ell |\Psi_{\ell m}|^2}} \ .$$

- We can also predict the expected SNR of the unfiltered field:

$$\Gamma_{\rm orig} = \frac{A \sum_{\ell m} \sqrt{\frac{2\ell+1}{4\pi} \frac{(\ell-m)!}{(\ell+m)!}} \, \tau_{\ell m}}{\sqrt{\sum_\ell \frac{2\ell+1}{4\pi} C_\ell}} \ .$$

Theoretical signal-to-noise ratios (SNRs)

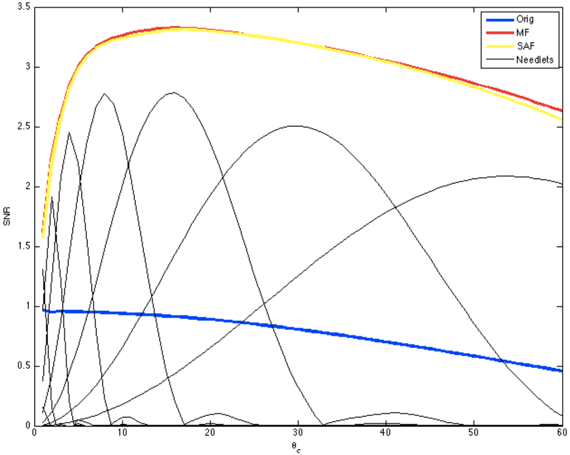

Figure: Theoretical SNRs versus template size θ_{crit}.

Detection algorithm for bubble signatures of unknown size

- Consider a discrete set of candidate $\theta_{\rm crit}$ scales.
- Ensure grid sufficiently coarse that SNR not significantly hampered.

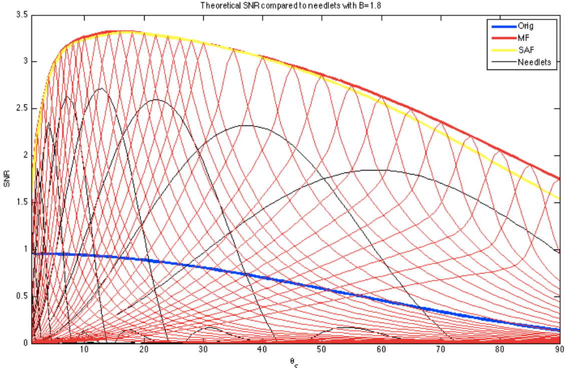

Figure: Theoretical SNRs for filters matched to given scale $\theta'_{\rm crit}$.

Detection algorithm for bubble signatures of unknown size

Bubble collision detection algorithm

1. Filter the sky with the matched filter for each scale (i.e. for each candidate θ_{crit}).
2. Compute significance maps for each filter scale, where the significance is given by the number of standard deviations that the filtered field deviates from the mean (3,000 Gaussian CMB simulations are used to determined the filtered field mean and variance).
3. Threshold the significance maps for each filter scale (the N_σ threshold for each filter will subsequently be calibrated from WMAP end-to-end simulations).
4. Find localised peaks in the thresholded significance maps for each filter scale.
5. Consider the local peak found at each scale. Look across adjacent scales and if a nearby region in an adjacent scale has a greater peak in the filtered field, then discard the current local peak. Otherwise retain the local peak as a detected source.
6. For all detected sources, estimate parameters of the source size, location and amplitude from the filter scale, peak position of the significance map and amplitude of the filtered field respectively.

Detection algorithm for bubble signatures of unknown size

Bubble collision detection algorithm

1. Filter the sky with the matched filter for each scale (i.e. for each candidate θ_{crit}).
2. Compute significance maps for each filter scale, where the significance is given by the number of standard deviations that the filtered field deviates from the mean (3,000 Gaussian CMB simulations are used to determined the filtered field mean and variance).
3. Threshold the significance maps for each filter scale (the N_σ threshold for each filter will subsequently be calibrated from WMAP end-to-end simulations).
4. Find localised peaks in the thresholded significance maps for each filter scale.
5. Consider the local peak found at each scale. Look across adjacent scales and if a nearby region in an adjacent scale has a greater peak in the filtered field, then discard the current local peak. Otherwise retain the local peak as a detected source.
6. For all detected sources, estimate parameters of the source size, location and amplitude from the filter scale, peak position of the significance map and amplitude of the filtered field respectively.

Detection algorithm for bubble signatures of unknown size

Bubble collision detection algorithm

1. Filter the sky with the matched filter for each scale (i.e. for each candidate $\theta_{\rm crit}$).
2. Compute significance maps for each filter scale, where the significance is given by the number of standard deviations that the filtered field deviates from the mean (3,000 Gaussian CMB simulations are used to determined the filtered field mean and variance).
3. Threshold the significance maps for each filter scale (the N_σ threshold for each filter will subsequently be calibrated from WMAP end-to-end simulations).
4. Find localised peaks in the thresholded significance maps for each filter scale.
5. Consider the local peak found at each scale. Look across adjacent scales and if a nearby region in an adjacent scale has a greater peak in the filtered field, then discard the current local peak. Otherwise retain the local peak as a detected source.
6. For all detected sources, estimate parameters of the source size, location and amplitude from the filter scale, peak position of the significance map and amplitude of the filtered field respectively.

Detection algorithm for bubble signatures of unknown size

Bubble collision detection algorithm

1. Filter the sky with the matched filter for each scale (i.e. for each candidate θ_{crit}).
2. Compute significance maps for each filter scale, where the significance is given by the number of standard deviations that the filtered field deviates from the mean (3,000 Gaussian CMB simulations are used to determined the filtered field mean and variance).
3. Threshold the significance maps for each filter scale (the N_σ threshold for each filter will subsequently be calibrated from WMAP end-to-end simulations).
4. Find localised peaks in the thresholded significance maps for each filter scale.
5. Consider the local peak found at each scale. Look across adjacent scales and if a nearby region in an adjacent scale has a greater peak in the filtered field, then discard the current local peak. Otherwise retain the local peak as a detected source.
6. For all detected sources, estimate parameters of the source size, location and amplitude from the filter scale, peak position of the significance map and amplitude of the filtered field respectively.

Detection algorithm for bubble signatures of unknown size

Bubble collision detection algorithm

1. Filter the sky with the matched filter for each scale (i.e. for each candidate θ_{crit}).
2. Compute significance maps for each filter scale, where the significance is given by the number of standard deviations that the filtered field deviates from the mean (3,000 Gaussian CMB simulations are used to determined the filtered field mean and variance).
3. Threshold the significance maps for each filter scale (the N_σ threshold for each filter will subsequently be calibrated from WMAP end-to-end simulations).
4. Find localised peaks in the thresholded significance maps for each filter scale.
5. Consider the local peak found at each scale. Look across adjacent scales and if a nearby region in an adjacent scale has a greater peak in the filtered field, then discard the current local peak. Otherwise retain the local peak as a detected source.
6. For all detected sources, estimate parameters of the source size, location and amplitude from the filter scale, peak position of the significance map and amplitude of the filtered field respectively.

Detection algorithm for bubble signatures of unknown size

Bubble collision detection algorithm

1. Filter the sky with the matched filter for each scale (i.e. for each candidate θ_{crit}).
2. Compute significance maps for each filter scale, where the significance is given by the number of standard deviations that the filtered field deviates from the mean (3,000 Gaussian CMB simulations are used to determined the filtered field mean and variance).
3. Threshold the significance maps for each filter scale (the N_σ threshold for each filter will subsequently be calibrated from WMAP end-to-end simulations).
4. Find localised peaks in the thresholded significance maps for each filter scale.
5. Consider the local peak found at each scale. Look across adjacent scales and if a nearby region in an adjacent scale has a greater peak in the filtered field, then discard the current local peak. Otherwise retain the local peak as a detected source.
6. For all detected sources, estimate parameters of the source size, location and amplitude from the filter scale, peak position of the significance map and amplitude of the filtered field respectively.

Candidate bubble collisions in WMAP 7-year observations

- Applied candidate bubble collision detection algorithm to WMAP W-band 7-year data.
- First calibrated N_σ thresholds on WMAP end-to-end simulations (without bubble collisions), resulting in 13 false detections (allow a manageable number of false detections since preprocessing).

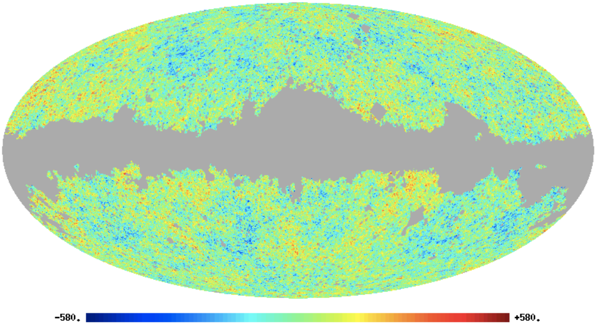

Figure: WMAP W-band 7-year data.

Candidate bubble collisions in WMAP 7-year observations

- Applied candidate bubble collision detection algorithm to WMAP W-band 7-year data.
- First calibrated N_σ thresholds on WMAP end-to-end simulations (without bubble collisions), resulting in 13 false detections (allow a manageable number of false detections since preprocessing).

16 candidate bubble collisions detected in WMAP 7-year data for follow-up analysis (8 new regions not detected previously)!

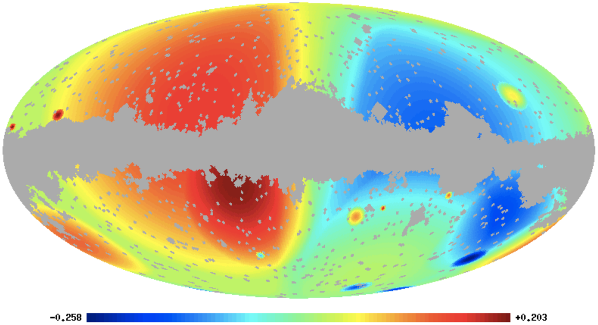

Figure: Candidate bubble collisions.

Candidate bubble collisions in WMAP 7-year observations

- Applied candidate bubble collision detection algorithm to WMAP W-band 7-year data.
- First calibrated N_σ thresholds on WMAP end-to-end simulations (without bubble collisions), resulting in 13 false detections (allow a manageable number of false detections since preprocessing).

16 candidate bubble collisions detected in WMAP 7-year data for follow-up analysis (8 new regions not detected previously)!

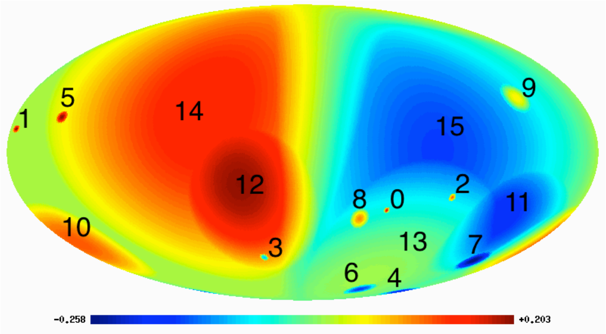

Figure: Candidate bubble collisions.

Summary

- Eternal inflation is well motivated and can lead to the creation of distinct bubble universes.
- Bubble collisions may have left observational signatures in the CMB.
- Bayesian object detection would provide a rigorous statistical analysis but is computationally intractable on current and forthcoming high-resolution CMB data-sets.
- Perform a preprocessing to detect candidate bubble collisions, followed by a local Bayesian analysis.
- Developed an optimal filter based preprocessing stage to exploit the knowledge of explicit bubble collision signatures.
- Provides an improvement in sensitivity over needlets by a factor of ~ 2.
- Detected 8 new candidate bubble collision signatures in WMAP 7-year data for follow-up analysis.
- **Observational evidence for eternal inflation?**

Recovered candidate bubble collision parameters

Label	Bubble collision parameters				Significance	Detected previously	Detected in other bands	
	z_0 (mK)	θ_0 ($^\circ$)	φ_0 ($^\circ$)	θ_{crit} ($^\circ$)			V-band	Q-band
0	0.24	119.0	304.5	1.5	4.25	N	Y	N
1	0.20	78.3	176.5	2	4.15	N	N	Y
2	0.20	112.3	264.4	2	4.08	Y	Y	Y
3	-0.19	145.1	33.0	2	4.05	Y	N	N
4	-0.17	169.0	187.5	3	4.26	Y	Y	Y
5	0.17	72.4	150.8	3	4.02	Y	Y	Y
6	-0.16	167.2	268.7	4	4.56	Y	Y	Y
7	-0.16	147.4	207.1	5	4.67	Y	Y	Y
8	0.15	123.2	321.3	5	4.43	Y	Y	Y
9	0.14	62.7	220.4	7	4.39	N	Y	Y
10	0.11	136.6	172.6	20	3.94	Y	Y	Y
11	-0.09	127.2	216.9	26	3.07	N	N	Y
12	0.09	116.3	31.6	35	3.33	N	Y	N
13	0.10	136.6	282.0	40	3.07	N	N	Y
14	0.15	69.6	62.6	85	3.03	N	Y	N
15	-0.16	88.5	277.7	90	3.11	N	Y	Y

Amplitude of the filtered field versus filter scale

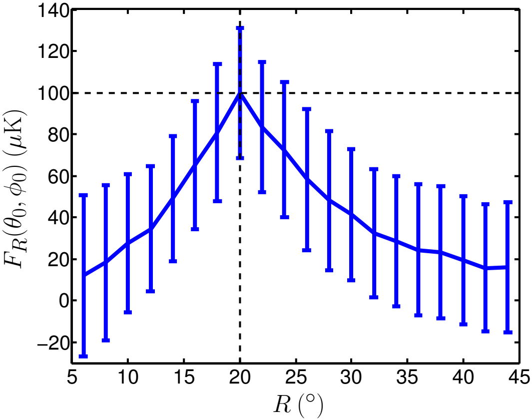

Figure: Amplitude of the filtered field at the position of a bubble collision signature versus the scale used to construct the corresponding MF.

Sensitivity

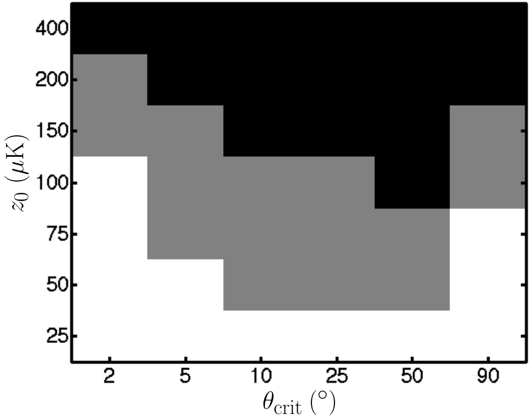

Figure: Exclusion (black) and sensitivity (grey) regions for the optimal-filter-based bubble collision detection algorithm. Bubble collision signatures that lie in exclusions regions would certainly be detected by the algorithm provided they were not significantly masked, while collision signatures that lie in sensitivity regions would be detected if they were in a favorable location on the sky.

Detection algorithm illustrated

- Embed bubble signatures at sizes $\theta_{\rm crit}^{\rm truth} \in \{10^\circ, 13^\circ, 20^\circ\}$ but consider discretised grid of $\theta_{\rm crit} \in \{5^\circ, 10^\circ, 20^\circ, 30^\circ\}$.

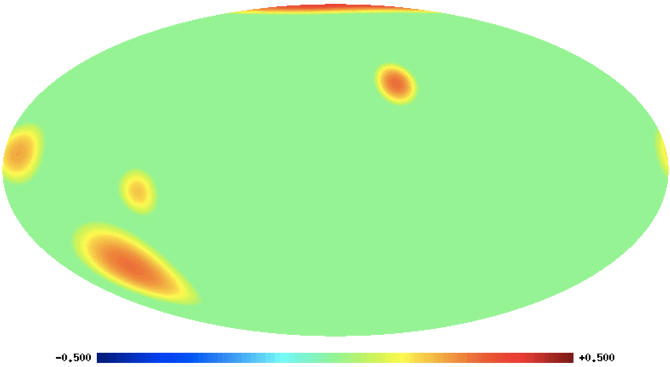

Figure: Embedded bubble collision signatures.

Detection algorithm illustrated

- Embed bubble signatures at sizes $\theta_{\text{crit}}^{\text{truth}} \in \{10^\circ, 13^\circ, 20^\circ\}$ but consider discretised grid of $\theta_{\text{crit}} \in \{5^\circ, 10^\circ, 20^\circ, 30^\circ\}$.

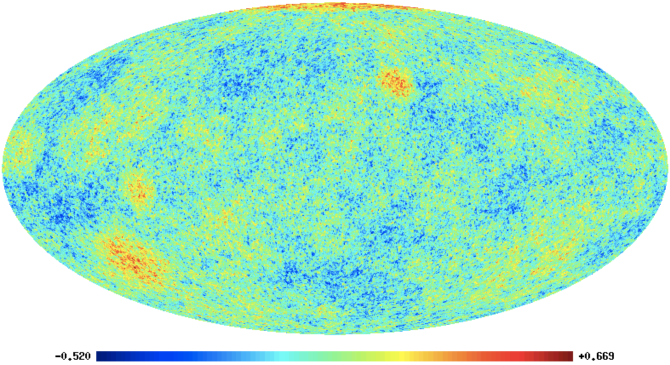

Figure: Simulated data.

Detection algorithm illustrated

- Embed bubble signatures at sizes $\theta_{\mathrm{crit}}^{\mathrm{truth}} \in \{10^\circ, 13^\circ, 20^\circ\}$ but consider discretised grid of $\theta_{\mathrm{crit}} \in \{5^\circ, 10^\circ, 20^\circ, 30^\circ\}$.

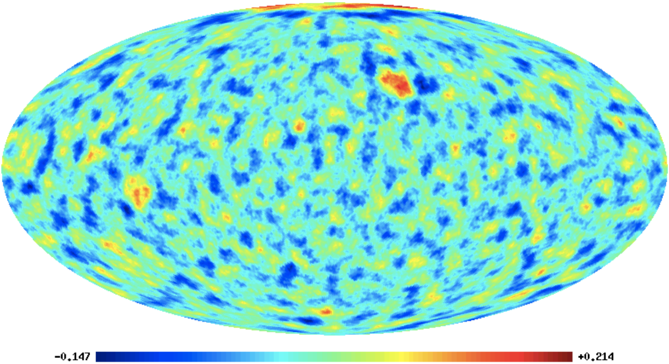

Figure: Filtered field for $\theta_{\mathrm{crit}} = 5^\circ$.

Detection algorithm illustrated

- Embed bubble signatures at sizes $\theta_{\text{crit}}^{\text{truth}} \in \{10^\circ, 13^\circ, 20^\circ\}$ but consider discretised grid of $\theta_{\text{crit}} \in \{5^\circ, 10^\circ, 20^\circ, 30^\circ\}$.

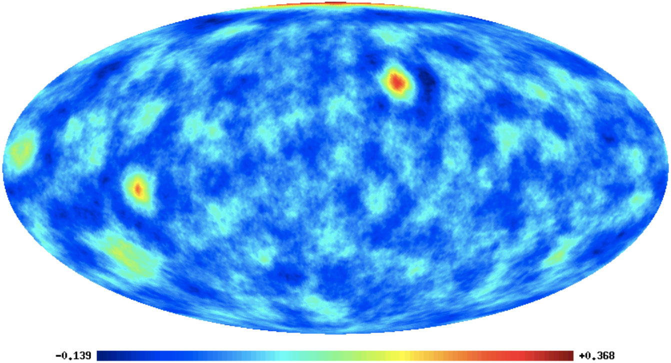

Figure: Filtered field for $\theta_{\text{crit}} = 10^\circ$.

Detection algorithm illustrated

- Embed bubble signatures at sizes $\theta_{\rm crit}^{\rm truth} \in \{10^\circ, 13^\circ, 20^\circ\}$ but consider discretised grid of $\theta_{\rm crit} \in \{5^\circ, 10^\circ, 20^\circ, 30^\circ\}$.

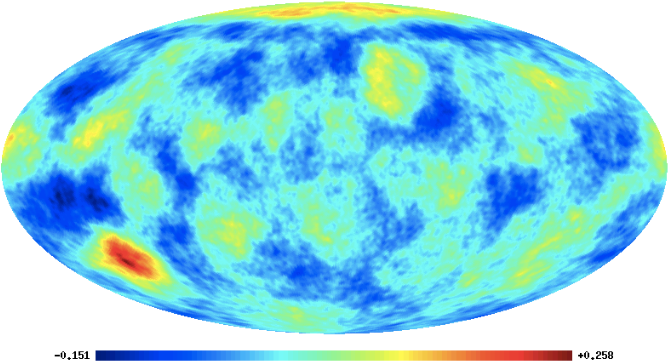

Figure: Filtered field for $\theta_{\rm crit} = 20^\circ$.

Detection algorithm illustrated

- Embed bubble signatures at sizes $\theta_{\rm crit}^{\rm truth} \in \{10^\circ, 13^\circ, 20^\circ\}$ but consider discretised grid of $\theta_{\rm crit} \in \{5^\circ, 10^\circ, 20^\circ, 30^\circ\}$.

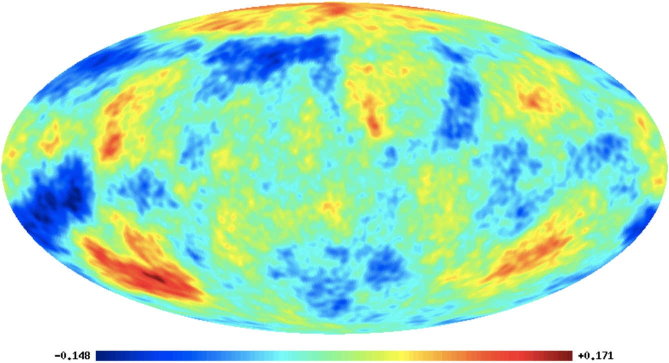

Figure: Filtered field for $\theta_{\rm crit} = 30^\circ$.

Detection algorithm illustrated

- Embed bubble signatures at sizes $\theta_{\text{crit}}^{\text{truth}} \in \{10^\circ, 13^\circ, 20^\circ\}$ but consider discretised grid of $\theta_{\text{crit}} \in \{5^\circ, 10^\circ, 20^\circ, 30^\circ\}$.

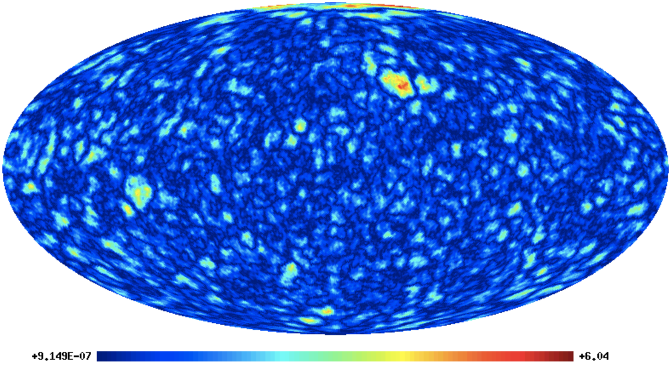

Figure: Significance map for $\theta_{\text{crit}} = 5^\circ$.

Detection algorithm illustrated

- Embed bubble signatures at sizes $\theta_{\text{crit}}^{\text{truth}} \in \{10^\circ, 13^\circ, 20^\circ\}$ but consider discretised grid of $\theta_{\text{crit}} \in \{5^\circ, 10^\circ, 20^\circ, 30^\circ\}$.

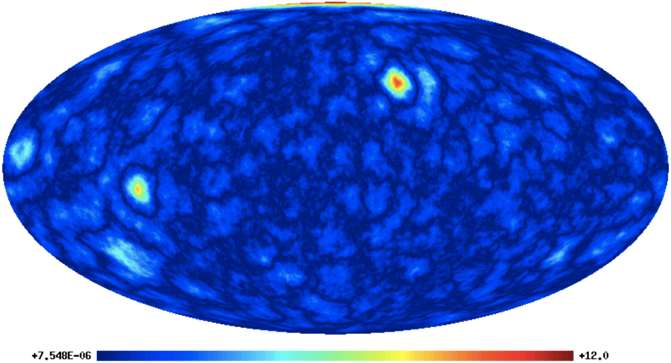

Figure: Significance map for $\theta_{\text{crit}} = 10^\circ$.

Detection algorithm illustrated

- Embed bubble signatures at sizes $\theta_{\rm crit}^{\rm truth} \in \{10^\circ, 13^\circ, 20^\circ\}$ but consider discretised grid of $\theta_{\rm crit} \in \{5^\circ, 10^\circ, 20^\circ, 30^\circ\}$.

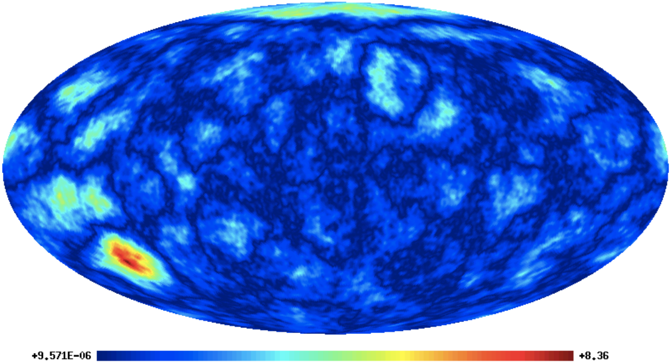

Figure: Significance map for $\theta_{\rm crit} = 20^\circ$.

Detection algorithm illustrated

- Embed bubble signatures at sizes $\theta_{\text{crit}}^{\text{truth}} \in \{10^\circ, 13^\circ, 20^\circ\}$ but consider discretised grid of $\theta_{\text{crit}} \in \{5^\circ, 10^\circ, 20^\circ, 30^\circ\}$.

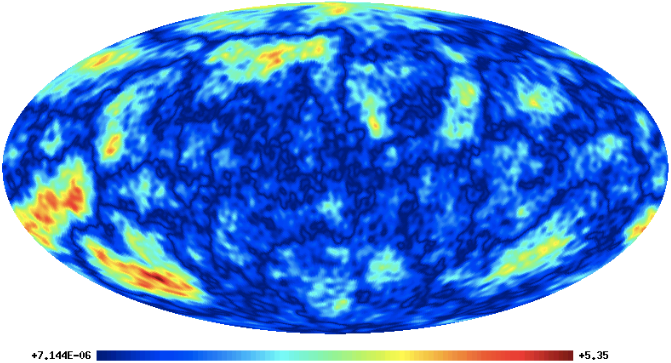

Figure: Significance map for $\theta_{\text{crit}} = 30^\circ$.

Detection algorithm illustrated

- Embed bubble signatures at sizes $\theta_{\rm crit}^{\rm truth} \in \{10^\circ, 13^\circ, 20^\circ\}$ but consider discretised grid of $\theta_{\rm crit} \in \{5^\circ, 10^\circ, 20^\circ, 30^\circ\}$.

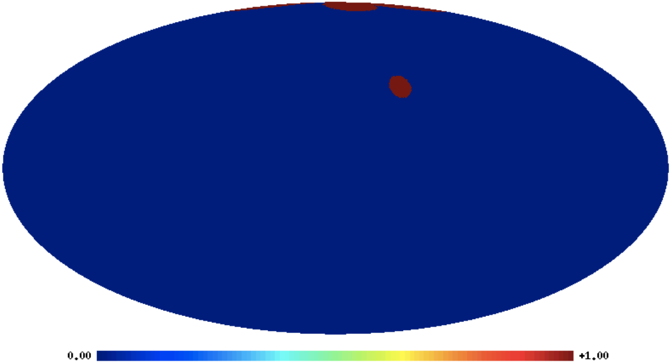

Figure: Detected regions for $\theta_{\rm crit} = 5^\circ$.

Detection algorithm illustrated

- Embed bubble signatures at sizes $\theta_{\rm crit}^{\rm truth} \in \{10^\circ, 13^\circ, 20^\circ\}$ but consider discretised grid of $\theta_{\rm crit} \in \{5^\circ, 10^\circ, 20^\circ, 30^\circ\}$.

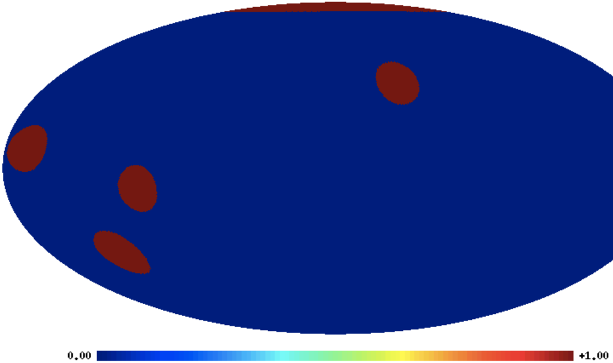

Figure: Detected regions for $\theta_{\rm crit} = 10^\circ$.

Detection algorithm illustrated

- Embed bubble signatures at sizes $\theta_{\text{crit}}^{\text{truth}} \in \{10^\circ, 13^\circ, 20^\circ\}$ but consider discretised grid of $\theta_{\text{crit}} \in \{5^\circ, 10^\circ, 20^\circ, 30^\circ\}$.

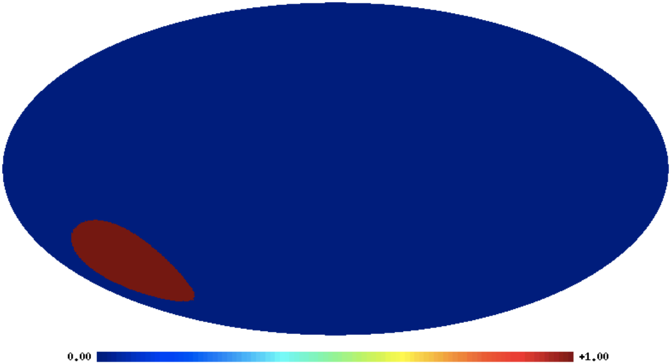

Figure: Detected regions for $\theta_{\text{crit}} = 20^\circ$.

Detection algorithm illustrated

- Embed bubble signatures at sizes $\theta_{\text{crit}}^{\text{truth}} \in \{10^\circ, 13^\circ, 20^\circ\}$ but consider discretised grid of $\theta_{\text{crit}} \in \{5^\circ, 10^\circ, 20^\circ, 30^\circ\}$.

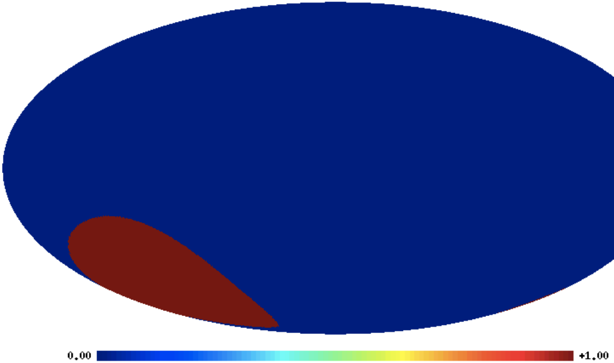

Figure: Detected regions for $\theta_{\text{crit}} = 30^\circ$.

Detection algorithm illustrated

- Embed bubble signatures at sizes $\theta_{\text{crit}}^{\text{truth}} \in \{10^\circ, 13^\circ, 20^\circ\}$ but consider discretised grid of $\theta_{\text{crit}} \in \{5^\circ, 10^\circ, 20^\circ, 30^\circ\}$.

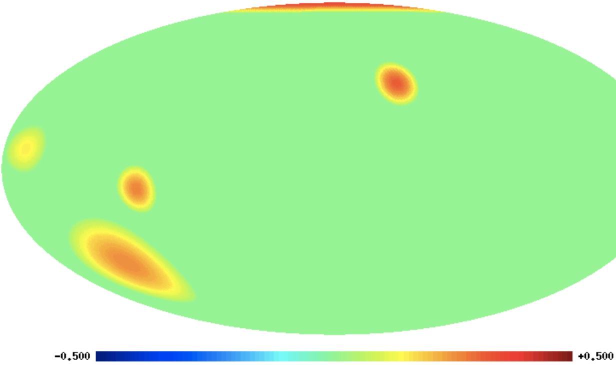

Figure: Detected regions.

Detection algorithm illustrated

- Embed bubble signatures at sizes $\theta_{\rm crit}^{\rm truth} \in \{10^\circ, 13^\circ, 20^\circ\}$ but consider discretised grid of $\theta_{\rm crit} \in \{5^\circ, 10^\circ, 20^\circ, 30^\circ\}$.

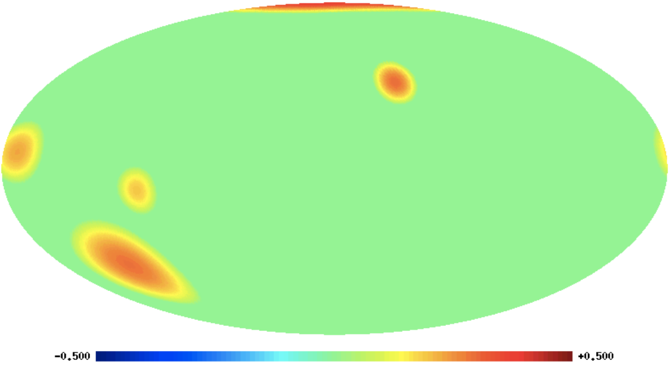

Figure: Ground truth.

Detection algorithm illustrated

- All objects detected successfully with no false detections (as expected for the intense bubble signatures considered in this illustration).
- Bubble collision template parameters estimated reasonably accurately for the preprocessing stage.
- Performed an extensive comparison and optimal filters found to be approximately twice as sensitive as needlets.

Source	Original size	Detected size	Original amplitude (mK)	Detected amplitude (mK)
1	10°	10°	0.34	0.36
2	10°	10°	0.30	0.31
3	13°	10°	0.23	0.15
4	10°	10°	0.19	0.24
5	20°	20°	0.29	0.25